RSC Advances

ROYAL SOCIETY OF CHEMISTRY

www.rsc.org/advances

Physicochemical Investigations of the Metal Complexes of L-Valine with Doubly Charged Ions of Nickel, Copper and Zinc: A Combined Experimental and Computational Approach

Shilpi Mandal, Gunajyoti Das* and Hassan Askari

Department of Chemistry, North Eastern Hill University, Shillong-793022, India
**Email: guna_das78@yahoo.co.in*

Abstract

Assessment of the intrinsic structural changes inflicted by metal coordination in the molecular geometries of the genetically encoded amino acids is of fundamental importance for proper characterization and understanding of the structure-function relationships of proteins and polypeptides. Efforts are being made here to investigate the coordination properties of L-valine as a potential metal-binding entity involving a combined solid state solvent free synthetic and computational approach. The metal complexes of L-valine with the divalent cations of nickel, copper and zinc are characterized by elemental analyses, molar conductance, EDAX-SEM, TEM, TG/DTA, infrared, electronic absorption, fluorescence and mass spectroscopy. Quantum chemical calculations carried out in gas and aqueous phase using B3LYP/6-311++G(d,p) level of theory provide valuable insights concerning the interaction enthalpies and Gibbs energies; vibrational and absorption spectra along with various other molecular and electronic properties of the metal complexes. Solvation effects are evident on the structure and stability of the metal complexes. Analysis of the geometrical parameters suggests significant changes in the molecular structure of L-valine as a result of metal binding. The harmonic frequencies furnished at B3LYP level are in good agreement with the earlier theoretical and experimental observations and well reflect the influence of the aqueous environment and identity of the metal ions on the structural and molecular properties of the complexes. The physical origin of the molecular interactions of L-Val with the metal ions has also been evaluated by performing EDA.

Keywords: Metal complexes of L-valine, Solvent free synthesis, DFT structural study, TD-DFT, HOMO/LUMO energies, Cation binding affinities, Theoretical vibrational frequencies.

1. Introduction

The genetic code encodes L-valine (L-Val) by means of a four-fold degenerate strategy using GUU, GUC, GUA and GUG codons. This essential α-amino acid plays a number of crucial chemical and bio-chemical roles in living organisms, besides assisting muscle metabolism and repair/growth of various tissues. In human body L-Val is involved in detoxification of ammonia and in maintaining nitrogen balance. Because of the hydrophobic nature of its branched side chain moiety, the hemoglobin is known to undergo abnormal aggregation. Over the past few decades, there have been numerous experiments referring to the infrared spectral features of DL-valine and some metal-valine complexes,[1] thermal properties of a series of metal-valine complexes[2] as well as stability constant of lanthanum(III) and samarium(III) complexes of valine in non-aqueous medium.[3] Report on synthesis and characterization of antimony and bismuth complexes of valine using a direct solid-solid reaction is also available in the literature.[4] On the other hand, *ab initio* studies have been carried out to characterize the gas-phase conformer of valine.[5] However, to the best of our knowledge, the literature survey reveals no reference on the utilization of a combined solid state experimental and quantum chemical investigation exploring the interactions of L-Val with the divalent metal ions of nickel, copper and zinc that can provide much deeper insights into the physicochemical properties of such metal complexes as well as the influence of metal coordination on the structural aspects of L-Val.

Metal ions are indispensable to our existence since the beginning of the formation of life on earth. The essential roles played by the metal cations in living systems range from hydrolysis processes to isomerizations, redox reactions, mechanisms of electron transfer, transport and storage as well as imparting magnetic properties to bio-molecules. The multi-stepped respiratory and photosynthetic processes are exclusively dependent on the metal containing proteins and enzymes. Some of the characteristic features that enable metal ions to perform such diverse range of functions include their small size, positive charge, electron acceptor ability, flexible coordination sphere, varying valence state and electron spin configuration.[6] The distribution and importance of bivalent metal cations of copper, nickel and zinc in various biological processes have been well documented in the literature.[7-10] The scintillating discovery of salt-induced peptide formation (SIPF) mechanism in 1989 has led to the realization that divalent transition metal ions like Cu(II) may have played vital roles in the formation of the first oligopeptides and peptides on the primitive earth from simple amino acid residues.[11-13] Computational studies have

revealed that metal cation electronic configuration can significantly modify the structural features of biologically important molecular systems such as glycylglycine dipeptide.[14] During the past few decades, low molecular weight metal complexes of canonical amino acids and their derivatives have attracted a great deal of interest from both experimental and theoretical stand-points by serving as model systems to imitate the active sites of various bio-macromolecular systems such as metalloproteins and metalloenzymes, and consequently providing deeper insights into their structure-function relationships. Such investigations are less complicated than those of the native macromolecules, and thus have emerged as a reliable approach to gather detailed information about the coordination behavior of amino acids as well as their derivatives towards biologically important metal ions. Exploring the relevant information concerning the fundamental nature of the metal-amino acid interactions is also becoming increasingly important in the field of rational design of metalloproteins[15,16] and in expanding the spectrum of properties of the engineered or de novo designed metalloproteins.[17,18]

In view of the growing concern throughout the world regarding the ever-increasing environmental degradation due to industrialization and other human activities, solid-state chemical synthesis provides a rewarding alternative way in the field of synthetic chemistry since it has the advantages of lack of pollution, low energy consumption, high efficiency and convenient operation.[19-21] Solid state chemistry is an interdisciplinary melding of chemistry, physics, engineering, and materials science that focuses on designing, synthesizing as well as characterization of structural and physicochemical properties of new chemical compounds. Solid-state synthetic method has been successfully employed in synthesis and characterization of several biologically significant metal complexes which are, otherwise, difficult to achieve by following the traditional synthetic methods or in presence of solvents.[21-23]

On the other hand, computational chemistry employing high-level computing has been regarded as the third pillar of modern scientific research, standing alongside the conventional methods of theory and experiment. Gas phase computational studies are useful in providing valuable information concerning the intrinsic coordinating properties of amino acids with metal ions free from solvent or crystal phase effects. However, since the vast majority of biochemical processes occur in an aqueous environment, it is of basic importance to determine the structural and molecular properties of biomolecules in aqueous environment. Also, proteins and polypeptides contain many charged or polar groups which interact strongly with polar solvents

like water and as a result the solvent effects of aqueous phase often play critical roles in modifying the gas phase structural features of biomolecules. It has now been widely acknowledged that computational techniques are indispensable in elucidating atomic level structural information about biologically active molecules owing to certain limitations of experimental techniques as pointed out in the literature.[24,25] Experimental investigations carried out in close conjunction with theoretical calculations constitute a more efficient way of assembling atomic level information about stability and structure-function relationships of bioactive molecules.[21,24]

The chief objective of this study is to investigate the coordination properties of L-Val as a potential metal-binding entity and report the results on the solid state synthesis and characterization of Cu(II), Ni(II) and Zn(II) complexes of L-Val. Co-precipitation method has also been employed to study the mode of interaction of L-Val with the above mentioned metal cations and to see whether the products formed in both the phases (solid and solvent) are the same. Theoretical calculations are performed in gas and aqueous phase using B3LYP level of theory in an attempt to examine the effects of metal coordination on the back-bone structural features of L-Val and geometry about its α-carbon atom. The interaction enthalpies (ΔH), Gibbs energies (ΔG), theoretically predicted vibrational spectra, rotational constants, dipole moments, computed UV-Visible spectra, partial atomic charges and HOMO/LUMO energies as well as their energy gaps of all the representative reaction species are also calculated and thoroughly analyzed. Fig. 1 schematically portrays the chemical structures and atom numbering assigned to L-Val and its bivalent metal complexes. The carbon atom C_2 is the α-carbon atom of L-Val while those in the metal complexes are denoted as C_2 or C_{2a}. This experimental study carried out in tandem with computational calculations is expected to provide the opportunity to gain knowledge of the coordination properties of L-Val to metal ions as well as the effects of metal coordination on the structural and molecular properties of L-Val at an atomic level. This in turn may help us to understand its presence and functional activities performed in the macromolecular context of real life systems and to synthesize a new generation of metalloproteins containing L-Val.

2. Experimental Section

2.1. Reagents

Copper(II) acetate monohydrate (Laboratory Reagent), Nickel(II) acetate tetrahydrate (Laboratory Reagent), Zinc(II) acetate dehydrate (Himedia), L-valine (Himedia) and the other reagents used in the experiments were analytical reagent grade obtained from commercial sources and were used without further purification.

2.2. Synthesis of Reaction Products

Grinding method: The hydrated forms of the metal acetates were converted to their anhydrous forms by drying at 110 ^{o}C.[21] The metal complexes of L-Val were prepared according to the method mentioned in literature,[21] where the metal acetates and L- Val were ground separately at room temperature for about 15 min in an agate mortar and pestle. Then the reagents were mixed in 1:2 molar ratio (Metal:Ligand) and ground again at room temperature for 70 min. The colour of the reactants changed immediately with strong acetic acid odors being discharged. The mixtures were ground for 1 hr and heated on water bath at 70^{o}C for 3 hr to accelerate the reactions. The process of grinding, pulverization and heating was repeated several times. The products were washed for several times with deionised water and absolute ethyl alcohol of analytical grade. Finally, these were placed in a vacuum desiccator at ambient temperature to vacuum dry for 12 hr.

Co-precipitation method: 25 mmol of L-Val was dissolved in 25 ml of pure methanol containing 25 mmol of NaOH. Solutions of the Metal(II) acetates (12.5 mmol) in methanol were added drop-wise to the mixture and the precipitates appeared immediately. After stirring the mixtures at room temperature for 2 hr, the precipitates were collected by filtration, washed with methanol and dried under vacuum to constant weight. The solid complexes obtained were then dried at 110 ^{o}C and stored in a desiccator.

2.3. Instrumentation

The complexes obtained by following the grinding and co-precipitation methods were analyzed for C, H, and N contents on PerkinElmer 2400 Series II CHN-OS Analyzer. The molar conductance values were measured in DMSO (10^{-3} M) solution using a coronation digital conductivity meter (cell constant = 1.0 cm^{-1}). Infrared spectra of all the reaction species were recorded in KBr discs on a BOMEM DA-8 FTIR spectrophotometer at 4000-400 cm^{-1}. The electronic absorption spectra of L-Val and its metal complexes were also recorded in DMSO

solution (10^{-3} M) on a Perkin Elmer lambda 25 UV/VIS spectrometer. The dehydration level of DMSO was 99%. Fluorescence spectra of the products synthesized by the solid state technique were measured using a PerkinElmer LS 55 Fluorescence Spectrometer. The thermogravimetric (TG) and differential thermal analysis (DTA) measurements were carried out for the reaction products obtained by following the grinding method in controlled nitrogen atmosphere on a Perkin-Elmer STA 6000 Simultaneous Thermal Analyser at temperature ranging from 40 to 800 °C at heating rate 20 °C/min. The EDAX-SEM micrographs for the Cu(II) complex of L-Val were obtained in a Jeol, JSM-6360 LV apparatus, using an accelerating voltage between 15–20 kV at different magnifications. TEM images were obtained on a JEOL-JEM-2100CX electron microscope operated at 200 kV without adding any contrast agent. The mass spectra of the metal complexes were recorded on a Water ZQ4000 Micromass Spectrometer in DMSO solution. Melting points of all the reaction species were also determined on an IkonTM Instrument.

3. Computational Details

The molecular geometries of L-Val, its metal complexes with divalent cations of nickel, copper and zinc as well as the other reaction species involved in the equation (1) (shown below) were subjected to full geometry optimization and vibrational frequency calculations in gas and aqueous phase using a polarizable continuum model (PCM)[26] at the B3LYP/6–311++G(d,p) level of theory[27,28] of Gaussian 03 and 09 programs.[29,30] Absence of any imaginary frequency value in the vibrational frequency calculations confirmed that all the optimized geometries were true minima. The accuracy of self-consistent reaction field (SCRF) model in predicting structure and energetics of biologically important molecules has already been well documented in literature.[31] Zero point energy (ZPE) corrections were applied to the total energies of all the representative reaction species using a correction factor 0.9877.[32] The vibrational frequencies extracted from the theoretical IR spectra of L-Val and its divalent metal complexes were scaled using appropriate correction factors;[32] 0.9679 for ν(O-H), ν(N-H) and ν(C-H) stretching frequencies while 1.01 for those vibrational modes that appear below 1800 cm^{-1}. Use of diffuse functions is important to take into account the relative diffuseness of lone pair of electrons when a molecule under investigation contains the same.[33] Polarization functions are useful in studying the structural aspects of a molecule where stereoelectronic effects may play an important role.[34]

The gas and aqueous phase interaction enthalpies ΔH (cation binding affinities) and Gibbs energies ΔG were calculated using the scheme mentioned below:

$$2(\text{L-Val}) + \text{M(ace)}_2 \longrightarrow \text{M(L-Val)}_2 + 2\text{Acetic acid} \quad \ldots\ldots\ldots\ldots (1)$$

Thus, ΔH or $\Delta G = [Et_{\text{products}}] - [Et_{\text{reactants}}]$,

where, M = Ni(II), Cu(II) or Ni(II); and Et_{products} and $Et_{\text{reactants}}$ are the sum of ZPE corrected total electronic or Gibbs energies of the products and reactants respectively. Single-point calculations were performed on the fully optimized structures of all the representative reaction species in gas and solvent phase (DMSO) using time dependent density functional theory (TD-DFT)[35-39] to obtain the theoretical λ_{max} values. To evaluate the physical origin of the molecular interactions of L-Val with the metal ions, Kitaura-Morokuma decomposition analysis[40,41] was performed on the B3LYP optimized geometries of Ni(L-Val)$_2$ and Zn(L-Val)$_2$ complexes at the RHF/6-31G(d) level as implemented in the GAMESS-US package.[42]

4. Results and discussion

4.1. Experimental Results

4.1.1. Interactions of L-Val with metal ions

When the anhydrous forms of the metal acetates were mixed individually with L-Val in 1:2 molar ratios by following the above mentioned solvent free method; the observed colour changes were as follows – light-green for (L-Val + Ni^{2+}), purplish-blue for (L-Val + Cu^{2+}) and creamy-white for (L-Val + Zn^{2+}) systems. The colourations of the precipitation formed during the co-precipitation method were also same as the above mentioned solid state systems. Table 1 lists the physical, molar conductivity and analytical data of all the reaction species.

4.1.2. Elemental Analysis and Molar conductance

The results of CHN-OS elemental analyses as well as the proposed formula for the synthesized complexes (presented in Table 1) are in good agreement with the expected stoichiometries of the complexes. As it is evident from Table 1, the conductivity values of the complexes in DMSO indicate their non-electrolytic nature suggesting that these complexes are neutral.[43,44]

4.1.3. Experimental Infrared spectra

It is well known that free amino acids exist as zwitterions in solvent and solid phases but on metal coordination they are converted to their non-zwitterionic forms.[45] The experimentally determined infrared spectra of L-Val and its metal complexes are reported in the Supplementary Information (SI), while some of the structurally significant infrared assignments are listed in Table 2. Comparison of the infrared assignments of the free L-Val molecule with those of the metal complexes confirms that no free ligand molecules were present after the grinding procedure. The experimental infrared spectral data on the asymmetric and symmetric ν(N-H) stretching frequencies of L-Val and its metal complexes suggest that the ν_{as}(N-H) and ν_s(N-H) frequency values of L-Val (observed at 3436 and 3133 cm^{-1} respectively) are blue-shifted in all the three metal complexes (3446-3469 and 3252-3298 cm^{-1} respectively). This indicates that the NH_3^+ function of free L-Val gets deprotonated and binds to the metal ion through its nitrogen atom.[45] Indication of metal coordination *via* the nitrogen atom of L-Val is also provided by the fact that the ν(C-N) stretching value of L-Val (observed at 1134 cm^{-1}) is red-shifted in its metal complexes (1085-1116 cm^{-1}). The appearance of new low intensity bands in the range of 454-477 cm^{-1} in all the metal complexes of L-Val, which can be assigned to ν(M-N) stretching frequencies,[46] also confirms that the nitrogen atom of L-Val is involved in metal coordination. On the other hand, $\nu_{as}(COO^-)$ stretching mode of L-Val that appears at 1598 cm^{-1} shifts to higher side of the frequency scale (up to 1637 cm^{-1}) in the metal complexes while the $\nu_s(COO^-)$ stretching frequency of L-Val (observed at 1417 cm^{-1}) shifts to lower side of the frequency scale in its metal complexes (1414-1387 cm^{-1}). These observations indicate that L-Val binds to the metal ions *via* its carboxylate group.[47] Table 2 also presents the separations (Δδ values) between the $\nu_{as}(COO^-)$ and $\nu_s(COO^-)$ stretching modes of L-Val and its three metal complexes which are indicative of the M-O bond strengths and provide evidence that the carboxylate groups bind to the metal ions in monodentate fashion.[48] The Δδ values of the metal complexes, ranging from 209 to 250 cm^{-1}, indicate that the M-O bonds possess significant covalent character.[46] The new low intensity bands at 540-617 cm^{-1} in all the three metal complexes, which can be assigned to ν(M-O) stretching frequencies,[46] also confirms that L-Val interacts with metal ions *via* its carboxylate group. The peaks appearing at 2923-2962 cm^{-1} can be assigned to $\nu(C_2–H)$ stretching modes of the reaction species. Thus, the experimental IR spectra of the reacting species furnish noticeable signatures indicating that L-Val binds to the metal ions in bi-dentate manner through its amino and carboxylate groups.

4.1.4. Electronic absorption and spectrofluorometric studies

The optical properties of L-Val and its metal complexes were studied using electronic absorption and fluorescence spectroscopy. The observed and calculated λ_{max} values of L-Val and its metal complexes are listed in Table 3 while their experimental absorption spectra are depicted in Fig. 2. The experimental UV-Vis spectra of the reacting species show characteristic peaks in the region 261-405 nm which can be attributed to π-π^* and n-π^* transitions. The spectra for the Ni(II) and Cu(II) complexes of L-Val show additional peaks at 611-632 nm respectively due to d-d transitions.[49] Such d-d transitions are not exhibited by the Zn(II) complex due to the completely filled d-orbital of Zn(II) ion.[50] A discussion on the comparison of theoretical and experimental absorption spectra has been offered in a succeeding section of this paper.

Thus, by considering the data presented in Table 1 to 3, it is reasonable to conclude that the reaction products obtained from both the methods are same. The complexes formed by the solid state method are further subjected to spectrofluorometric, thermal (TG/DTA) and mass spectral analysis as described in the following paragraphs.

The fluorescence spectrum of a given ligand molecule may differ from those of its metal complexes either due to the changes in the geometrical environments of the various functional groups present in the ligand upon metal coordination or by the nature of the chelating metal ions.[51] In general, transition metal ions are effective fluorescent quenchers[52] and the often reported quenching of ligand's fluorescence properties by transition metal ions during complex formation can be attributed to the processes such as magnetic perturbation, redox activity, and electronic energy transfer. The photoluminescence properties of L-Val and its metal complexes were recorded at room temperature in DMSO and the observed spectra are shown in Fig. 3. As listed in Table 4, the emission spectrum of the L-Val molecule excited at 261 nm shows an emission peak at 337 nm while those of the complexes, excited at 269-274 nm, are observed in the range of 331–337 nm. The results of the present study are in good agreement with previous experimental studies,[51,53] where it has been recognized that the degree of the fluorescence quenching increases with the decreasing number of d-orbital electrons in the electronic configurations of the coordinating transition metal ions.

4.1.5. Thermal and mass spectral analysis

The metal complexes of L-Val were subjected to thermal analysis using thermo-gravimetric (TG) and differential thermal analysis (DTA) techniques. The thermal analysis data of the three complexes are summarized in Table 5, while the TG/DTA curves of the complexes are reported in the SI. The complexes do not show any weight loss in the range 160-180 °C indicating the absence of water molecules in the coordination sphere of the metal complexes.[54] The TGA curves indicate that the three complexes are thermally stable up to nearly 218-221 °C above which, i.e. between 218-482 °C, the mass loss steps begin and most of the organic parts of the metal complexes are lost during this period. This sharp decomposition period brings about 75% weight loss for the Ni(II) complex while 73% for each of the Cu(II) and Zn(II) complexes; and leads to complete formation of their corresponding oxides. The DTA curves of the metal complexes also show similar behavior that corresponds to the TGA curves; the small peaks at the range of 312-328 °C which could be attributed to melting of the complexes.

The mass spectra of the solid state products were recorded at room temperature (depicted in Fig. S4 of the SI), and they are used to compare the stoichiometric composition of the metal complexes of L-Val. The molecular ion peak for the Ni(II) complex observed at 291 *m/z* confirms the [ML_2] type stoichiometry of the metal chelates which is also supported by the mass spectra of the other two complexes. The Cu(II) complex shows molecular ion peak at 295 *m/z* which seems to lose four methyl groups (CH_3) giving an ion at 235 *m/z*. This ion further disintegrates losing two amino groups (NH_2) and results a peak at 203 *m/z*. The mass spectrum of the Zn(II) complex shows molecular ion peak at 297 *m/z* and the subsequent weight loss process that results the two peaks at 237 and 205 *m/z* can be similarly explained to that of the Cu(II) complex.

4.1.6. EDAX, SEM and TEM images

Finally, we report the energy-dispersive X-ray analysis (EDAX), scanning electron microscopy (SEM) and transmission electron microscopy (TEM) images of the Cu(L-Val)$_2$ complex prepared by following the solid state grinding procedure that provide valuable information concerning the chemical composition, surface morphology and particle size of the L-Val metal complexes. Fig. 4 and 5 portray the EDAX spectrum and SEM morphology of the gold coated sample of the Cu(L-Val)$_2$ complex respectively. The EDAX image confirms the existence of copper and purity of the complex while the SEM photograph displays a uniform and homogeneous matrix of the

synthesized complex with particle size ranging from 10 to 15 nm. It is difficult to know the exact composition of a given sample from the EDAX images since EDAX gives only surface analysis but not a detailed description of embedded particles. Fig. 6 represents the TEM micrographs of the Cu(L-Val)$_2$ complex which provides visual information regarding the amorphous nature of the sample with particle size ranging from 5.41 to 19.51 nm.

4.2. Computational Results

4.2.1. Structural and molecular properties

Zn(II) ions are known to prefer tetrahedral binding sites while interacting with proteins under the physiological conditions.[55,56] The vacant s orbital of Zn(II) ion enables it to establish strong interactions with a host of ligands while the filled d orbital (d^{10}) profoundly influences the coordination chemistry of the Zn(II) ion. Unlike other transition metal ions, for example Ni(II) and Cu(II) ions which possess partially filled d shells i.e. d^8 and d^9 respectively, the Zn(II) ion does not lose ligand field stabilization energy (LFSE) while going from an octahedral M(H_2O)$_6$ arrangement in solution to a tetrahedral site in a protein due to its filled d orbital.[56] Complementing the above rationale the Ni(L-Val)$_2$ and Cu(L-Val)$_2$ complexes assume nearly square-planar type of geometries, while the Zn(L-Val)$_2$ complex gives a nearly tetrahedral geometry in both gas and aqueous phases. The aqueous phase optimized structures of L-Val (the non-ionic structure is taken from gas phase calculations) and its metal complexes are depicted in Fig. 7. The zero-point vibrational energies (ZPVE), total electronic energies (E) and Gibbs free energies (G) as well as their respective ZPVE corrected values, E_{corr} and G_{corr}, of L-Val and it metal complexes calculated in gas and aqueous phase are listed in Table S1 of the SI. The gas and aqueous phase data on interaction enthalpies (ΔH), Gibbs energies (ΔG), dipole moments, rotational constants and HOMO/LUMO energy gaps of all the representative reaction species are presented in Table 6. The negative values of interaction enthalpies (-80.23 to -43.50 kcal/mol in gas phase and -66.36 to -27.33 kcal/mol in aqueous phase) and Gibbs energies (-74.74 to -38.87 kcal/mol in gas phase and -64.18 to -26.49 kcal/mol in aqueous phase) for all the three complexes indicate that the interactions of metal ions with L-Val lowers the total electronic energies of the metal complexes, and that the complexes are thermodynamically stable. In view of the B3LYP predicted data on the energetics of the metal complexes the metal binding affinity order of L-Val emerges as Ni(II)>Cu(II)>Zn(II) in aqueous phase. However, in gas phase the

Zn(II) complex is predicted to be more stable than the Cu(II) complex by narrow margins of 1.32 and 2.2 kcal/mol in terms of interaction enthalpy and Gibbs energy respectively. This could probably be attributed to the fact that the gas phase intramolecular H-bond combination which benefits the thermodynamic stability of the $Zn(L\text{-}Val)_2$ complex gets significantly weakened due to the solvation effects of the aqueous environment and consequently affects the energetics of the $Zn(L\text{-}Val)_2$ complex in aqueous phase. The gas and aqueous phase data on the total dipole moments of L-Val and its metal complexes, listed Table 6, reveals that the $Zn(L\text{-}Val)_2$ complex with tetrahedral geometry shows higher values of dipole moments (7.147 D in gas phase and 11.469 D in aqueous phase) while the square-planar $Ni(L\text{-}Val)_2$ and $Cu(L\text{-}Val)_2$ complexes show lower values of dipole moments (0.423 D to 0.661 D in gas phase and 0.580 D to 1.144 D in aqueous phase). The larger dipole moment value of the $Zn(L\text{-}Val)_2$ complex indicates that this complex has greater polar character and consequently possesses greater affinity to polar solvents. On the other hand, the accuracy of DFT method in predicting the rotational constants of conformers of some aliphatic amino acids has been discussed in the literature.[57] In the absence of any experimental data on rotational constants and dipole moments, these theoretically predicted gas and aqueous phase values may assist future experimentalists. Table 6 also represents the gas and aqueous phase results on the gaps between the highest occupied molecular orbital (HOMO) and lowest unoccupied molecular orbital (LUMO) energies of all the reaction species, while Fig. 8 depicts the 3D plots of the frontier orbitals for the three metal complexes. It is Fukui who, for the first time, pointed out the important roles played by HOMO and LUMO in governing the course of a chemical reaction.[58] The predicted energy gap for L-Val in gas and aqueous phase are 6.451 and 6.567 eV respectively, while those in the complexes range from 4.803-5.541 eV in gas phase and 4.840-6.373 eV in aqueous phase. In line with the previous theoretical observations,[59] the data furnished by this DFT study suggests that the HOMO–LUMO energy gaps of all the metal complexes increase in the presence of a solvent with high dielectric constant compared to those in gas phase. The partial atomic charges in L-Val and its metal complexes obtained from different methodologies viz. Natural Bond Orbitals (NBO) analysis and Merz–Kollman Electrostatic Potential are gathered in Table S2 of SI alongside the oldest definition of atomic charges, the Mulliken partial charges. The molecular electrostatic potential (MEP) charge distribution of the representative reaction species calculated at B3LYP/6-311++G(d,p) level has been depicted in Fig. 9. The high electron density, represented by red colour, is related to regions

of high electrophilic reactivity whereas the blue coloured portions indicate the electron deficient i.e. nucleophilic sites in the complexes. The study of MEP charge distribution in a molecular system is important since it can provide valuable insights regarding the presence of inter- and intramolecular H-bond interactions, the reactivity of different atomic sites towards electrophilic and nucleophilic attack as well as the vibrational spectral properties of the molecule. Additionally, the natural population analysis (NPA) charges provide valuable information regarding the influence of the identity of the metal ions on the atomic charge changes in the L-Val molecule as a result of metal coordination. For example, the partial charges on the atoms related to the amino and carboxylate groups as well as the α-carbon atom of the ligand molecule are changed considerably depending upon the identity of the coordinating metal ion. It is also apparent from the NPA charges that the Ni(II) ion with its d^8 configuration significantly reduces the charge densities on the amino and carboxylate groups of L-Val compared to the other two metal ions, thus showing strongest Lewis acid character amongst the three metal ions considered in this study. The energy decomposition analysis (EDA) results on the Ni(L-Val)$_2$ and Zn(L-Val)$_2$ complexes, reported in the SI, are also consistent with our experimental observations where we have recognized that the M-O bonds in the metal complexes of L-Val possess significant covalent character.

Atomic level structural information obtained from quantum chemical calculations regarding the effects of metal coordination on the geometrical parameters linked to the back-bone structural features and geometry of the α-carbon atoms of canonical amino acids are crucial for the purpose of supporting or refuting the existing theories devoted to protein structure prediction. Such information is also important for obtaining accurate geometrical force field parameters for semiempirical or molecular mechanics simulations of proteins and other bio-macromolecules.[60] The predicted gas and aqueous phase bond length values of some structurally significant bonds of free L-Val and its metal complexes are assembled in Table 7. The effects of metal ion coordination on the geometry about the C_2 α-carbon atom of L-Val have been monitored by considering three bonds, namely C_2–C_1, C_2–C_3 and C_2–N_6. A maximum deviation up to 0.023 Å in gas phase and 0.027 Å in aqueous phase in the C_2–N_6 bond of Zn(L-Val)$_2$ from that of the free L-Val molecule indicates that the geometry around the α-carbon atom of L-Val is affected due to metal ion coordination *via* its O- and N-atoms. Considerable change in the bond length value is also evident in case of the C_1-O_7 bond where the bond length value deviates up to a maximum of

0.042 Å in gas phase and 0.039 Å in aqueous phase. On the other hand, the predicted bond length values of the M-O and M-N bonds of the metal complexes suggest that they are relatively shorter in the Ni(L-Val)$_2$ complex (in aqueous phase M-O is 1.863 Å and M-N is 1.925 Å) compared to those in the Cu(L-Val)$_2$ and Zn(L-Val)$_2$ complexes (M-O bonds range from 1.942 to 1.993 Å and M-N bonds range 2.019 to 2.113 Å in aqueous phase). The M-O and M-N bond length values furnished in this study are in good agreement with the previous theoretical results regarding the 1:1 (Metal:Ligand) complexes of Ni(II), Cu(II) and Zn(II) ions with the non-ionic arginine molecule.[61] Table 7 also collects the gas and aqueous phase data on the Wiberg bond indices[62] for the M-O and M-N bonds of the metal complexes. The Wiberg bond indices are helpful in estimating the bond order and, hence, the bond strength between two chemically bonded atoms. It is evident that the predicted bond indices of M-O and M-N bonds of the Ni(L-Val)$_2$ complex are higher than those of the other two complexes. Thus, extending a fine corroboration to the data on the M-O and M-N bond length values as well as the thermodynamic parameters (ΔH and ΔG) of the metal complexes, the Wiberg bond indices for the M-O and M-N bonds also indicate that the interaction of L-Val with Ni(II) ion results the most stable metal complex out of the three metal ions considered in this study. Table 8 gathers the gas and aqueous phase values of the bond angles considered to monitor the effects of metal coordination on the geometry about the α-carbon atom, C-atom of the carboxylic and N-atom of the amino group of the L-Val molecule. The α-carbon atoms of the amino acids are sp3 hybridized and therefore the ideal bond angle should be 109.5°, however, this is not expected due to their chiral nature. Out of the three bond angles related to the α-carbon geometry, namely N_6–C_2–C_1, N_6–C_2–C_3 and C_1–C_2–C_3, the N_6–C_2–C_1 angle of the Zn(L-Val)$_2$ complex shows a maximum deviation up to 4.1° in gas phase and 6.7° in aqueous phase from that of the free L-Val reflecting the influence of metal coordination on the α-carbon geometry of L-Val. On the other hand, with a maximum deviation up to 7.1° in gas phase and 5.6° in aqueous phase for the C_2-C_1-O_8 angle of the Zn(L-Val)$_2$ complex, the geometry about the C-atom of the carboxylic group is also significantly affected. The geometry about the N-atom of the amino group also shows a maximum deviation up to 9.3° in aqueous phase while the other parts of the L-Val molecule remains more or less unaltered upon metal coordination. Table 9 lists the values of seven structurally significant backbone dihedral angles of L-Val and its metal complexes in both the phases. These data suggest that the structural aspects of the zwitterionic form of L-Val differ significantly from those of its non-ionic form. It

is also evident from Table 9 that compared to the non-ionic L-Val molecule the zwitterionic L-Val requires to undergo greater structural readjustments to be able to interact with metal ions *via* its N- and O-atoms, for example, the O_7-C_1-C_2-C_3 angle of the Cu(L-Val)$_2$ complex shows a maximum deviation of 58.8° from that of the zwitterionic L-Val. On the other hand, the N_6-C_2-C_3-O_5 dihedral angle of the Zn(L-Val)$_2$ complex deviates up to a maximum magnitude of 103.0° in gas phase and 107.5° in aqueous from that of free L-Val reflecting the amount of internal structural changes which the L-Val molecule has to go through while coordinating with the Zn(II) ion.

4.2.2. Theoretical vibrational spectra

The gas and aqueous phase vibrational spectra of all the reaction species were calculated at B3LYP/6–311++G(d,p) level to analyze the structural changes induced due to metal ion coordination in the L-Val molecule. The calculated quantum chemical vibrational frequencies are usually larger than their corresponding experimental values,[63] and such discrepancies have been attributed to the neglect of anharmonicity effects in theoretical treatments, incomplete incorporation of electron correlation and the use of finite basis sets. Nevertheless, the predicted harmonic frequencies of L-Val and its metal complexes provide valuable information contributing to the understanding of the effects of metal binding and influence of solvation on their structural and molecular properties. Moreover, it is well established that the vibrational frequencies shift invariably toward the lower side of frequency scale corresponding to the presence of intramolecular H-bond interactions in a given molecular system.[64] Thus, the theoretical spectra are expected to help us further in analyzing the existence and nature of the intramolecular H-bonds in the metal complexes. The accuracy of B3LYP functional in reproducing the experimental vibrational modes has been well discussed in the literature.[65] The L-Val molecule, in both zwitterionic and non-ionic forms, has a total of 51 normal modes of vibration while each of the metal complexes possesses a total of 105 modes. Table 2 lists the gas and aqueous phase values of some of the structurally important frequency and intensity values (given in parentheses) of the representative reaction species while their theoretical infrared spectra are reported in the SI (scaled with a correction factor 0.955). It is clear from the predicted IR data that some vibrational modes remain relatively unchanged corresponding to the structural changes in the L-Val molecule due to metal coordination while some are very sensitive to even

small structural changes, and consequently leave noticeable signatures in the IR spectra. For example, the ν_{as}(N-H), ν_s(N-H), ν(C_2-H), ν_{as}(COO^-), ν_s(COO^-) and ν(C-O) stretching frequencies of the metal complexes differ appreciably from those of the free L-Val molecule which can be attributed to the geometry changes around the N-atom of the amino group, α-carbon atom and the C-atom of the carboxylic group of L-Val upon metal ion coordination. The theoretically predicted frequency shifts of the ν_{as}(N-H), ν_s(N-H), ν_{as}(COO^-) and ν_s(COO^-) modes of L-Val after metal coordination are in good agreement with their corresponding experimentally observed values. The calculated frequencies of ν(M-O) and ν(M-N) modes are also complementary to the experimentally observed ones. On the other hand, the significant lowering in the ν(O-H) stretch frequency of the non-ionic L-Val well reflects the influence of intramolecular H-bond interactions in shifting the frequency values toward the lower side of the frequency scale. Thus, it reasonable to conclude that B3LYP hybrid functional in combination with 6-311++G(d,p) basis set performs well in reproducing the experimental vibrational frequencies as well as in describing the vibrational spectroscopy of the biologically relevant molecules.

4.2.3. Comparison of predicted and experimental UV-Vis spectra

The gas and solvent phase (DMSO) theoretical electronic absorption spectra of L-Val and its metal complexes calculated using TD-DFT level of theory show characteristic λ_{max} values around 210-623 nm (listed in Table 3). The accuracy of TD-DFT method in predicting theoretical UV-Vis spectra has been explained in the literature.[66] The occurrence of d-d transitions, λ_{max} values around 551-623 nm, only in the cases of Cu(II) and Ni(II) complexes of L-Val is well reproduced in our TD-DFT calculations.

5. Concluding remarks

The current work reports the results on the synthesis and characterization of Ni(II), Cu(II) and Zn(II) complexes of L-Val by following two synthetic methods; (a) solvent free solid state grinding method and (b) co-precipitation method. Characterization of the complexes by elemental analyses, molar conductance, EDAX-SEM, TEM, TG/DTA, infrared, electronic absorption, fluorescence and mass spectroscopy reveals that the products formed by following both the methods are same. The metal ions bind to L-Val in 1:2 molar ratio (Metal:Ligand) *via* its O- and N-atoms of the carboxylic and amino groups respectively. The ν_{as}(N-H) and ν_s(N-H)

stretch frequencies of L-Val are shifted to higher wave number after complex formation, which suggests that the NH_3^+ group of free L-Val gets deprotonated and binds to the metal ion through its nitrogen atom. The difference between $\nu_{as}(COO^-)$ and $\nu_s(COO^-)$ stretches for L-Val and its metal complexes provide evidence that the carboxylate group binds to the metal ion in monodentate fashion. The TG/DTA curves indicate that the metal complexes are thermally stable up to about 218 °C. The UV-Vis spectra of the Ni(II) and Cu(II) complexes show additional peaks at 611-632 nm due to d-d transitions, while such d-d transitions are not exhibited by the $Zn(L\text{-}Val)_2$ complex due to completely filled d-orbital of Zn(II) ion. DFT calculations at B3LYP/6-311++G(d,p) level of theory were carried out in an attempt to investigate the physicochemical properties of the metal complexes and the effects of metal coordination on the structural features of L-Val. The thermodynamic stabilities of the metal complexes are reflected by their negative values of ΔH and ΔG. The molecular properties of the metal complexes are analyzed in view of their gas and aqueous phase data on computed harmonic frequencies, UV-Vis spectra, dipole moments, rotational constants, wiberg bond indices, partial atomic charges as well as HOMO/LUMO energies and their energy gaps. Metal ion coordination modifies the geometry about the α-carbon atom, C-atom of the carboxylic and N-atom of the amino group of L-Val. The results furnished by this DFT study reveals that B3LYP hybrid functional in combination with 6-311++G(d,p) basis set performs well in reproducing the experimental results.

Acknowledgments

Financial assistance from the Special Assistance Program of the University Grants Commission, New Delhi, India, to the Department of Chemistry, N.E.H.U., is gratefully acknowledged. The analytical services provided by SAIF, N.E.H.U. are highly appreciated. S.M. is also grateful to the University Grants Commission, Government of India, New Delhi, for financial assistance through a research fellowship.

References

1. I. Nakagawa, R. J. Hooper, J. L. Walter and T. J. Lane, *Spectrochimica Acta,* 1966, **21**, 1-14.

2. M. Tomassetti, E. Cardarelli, R. Curini and G. D'ascenzo*, Thermochimica acta*, 1987, **113**, 243-255.

3. M. M. Suvarna, V. S. Panse, U. P. Fulwadva and P. K. Jadhav, *Asian J. Chem.,* 1995, **7(3),** 459-499.

4. J. G. Shao, Y. X. Yang, B.W. Li, L. P. Zhang, Y. R. Chen and X. L. Liu, *J. Ther. Anal. Cal.,* 2009, **96 (1),** 277–285.

5. S. Shirazian and S. Gronert, *J. Mol. Struct. (Theochem.),* 1997, **397**, 107-112.

6. T. Dudev and C. Lim, *Annu. Rev. Biophys.*, 2008, **39**, 97–116.

7. J. J. R. Frausto da Silva and R. J. P. Williams, The biological chemistry of the elements. Claredon Press, Oxford, 1991.

8. I. Bertini, A. Sigel and H. Sigel, Eds. Handbook on Metalloproteins; Marcel Dekker: New York, 2001.

9. T. Dudev and C. Lim, *Chem. Rev.*, 2003, **103**, 773-787.

10. D. W. Christianson and J. D. Cox, *Annu. Rev. Biochem.*, 1999, **68**, 33-57.

11. P. M. Kroneck, V. Vortisch and P. Hemmerich, *Eur. J. Biochem. IUY,* 1980, **12**, 603-612.

12. B. M. Rode, *Peptides*, 1999, **20**, 773–786.

13. B. M. Rode, J. Bujdak and A. H. Eder, *Trends Inorg. Chem.*, 1993, **3**, 45-62.

14. E. Constantino, A. Rimola, L. Rodriguez-Santiago and M. Sodupe, *New J. Chem.*, 2005, 29, 1585-1593.

15. W. F. DeGrado, C. M. Summa, V. Pavone, F. Nastri and A. Lombardi, *Annu. Rev. Biochem.,* 1999, **68**, 779–819.

16. Y. Lu, S. M. Berry and T. D. Pfister, *Chem. Rev.*, 2001, **101**, 3047–3080.

17. Y. Lu, *Curr. Op. Chem. Biol.,* 2005, **9**, 118–126.

18. J. Xie, W. Liu and P. G. Schultz, *Angew. Chem. Int. Ed.*, 2007, **46**, 9239-9242.

19. A. L. Garay, A. Pichon and S. L. James, *Chem. Soc. Rev.*, 2007, **36**, 846-855.

20. X. Q. Xin and L. M. Zheng, *J. Solid State Chem.*, 1993, **106**, 451-456.

21. S. Mandal, G. Das and H. Askari, *Struct. Chem.,* 2014, **25**, 43–51.

22. H. Koshima, D. Matsushige, M. Miyauchi and J. Fujita, *Tetrahedron,* 2000, **56**, 6845-6852.

23. T. Shimo, T. Uezono, T. Obata, M. Yasutake, T. Shinmyozu and K. Somekawa, *Tetrahedron,* 2002, **58**, 6111-6116.

24. M. R. Wormald, A. J. Petrescu, Y. Pao, A. Glithero, T. Elliott and R. A. Dwek, *Chem. Rev.*, 2002, **102(2),** 371-386.

25. N. Foloppe, B. Hartmann, L. Nilsson and A. D. Jr. MacKerell, *Biophys. J.*, 2002, **82**, 1554-1569.

26. S. Miertus, E. Scrocco and J. Tomasi, *Chem. Phys.*,1981, **55(1),** 117-129.

27. A. D. Becke, *J. Chem. Phys.*, 1993, **98**, 5648–5652.

28. C. Lee, W. Yang and R. G. Parr, *Phys. Rev. B*, 1988, **37**, 785–789.

29. M. J. Frisch, et al, Gaussian 03, Revision D.01 Gaussian Inc, Wallingford, CT, 2004.

30. M. J. Frisch, et al, Gaussian 09, Revision D02. Wallingford, CT: Gaussian, 2009.

31. I. R. Gould and I. H. Hillier, *J. Chem. Soc., Chem. Commun.,* 1993, 951-952.

32. M. P. Andersson and P. Uvdal, *J. Phys. Chem. A*, 2005, **109**, 2937-2941.

33. J. B. Foresman and A. Frisch, Exploring chemistry with electronic structure methods, 2nd edition, Gaussian, Inc. Pittsburgh, PA, 1996.

34. F. Freeman and K. T. Le, *J. Phys. Chem. A*, 2003, **107**, 2908-2918.

35. R. Bauernschmitt and R. Ahlrichs, *Chem. Phys. Lett.*, 1996, **256**, 454-464.

36. M. E. Casida, C. Jamorski, K. C. Casida and D. R. J. Salahub, *J. Chem. Phys.*, 1998, **108**, 4439-4449.

37. M. A. L. Marques and E. K. U. Gross, *Annual Review of Physical Chemistry*, 2004, **55**, 427-455.

38. E. Runge and E. K. U. Gross, *Phys. Rev. Lett.*, 1984, **52**, 997-1000.

39. R. E. Stratmann, G. E. Scuseria and M. J. Frisch, *J. Chem. Phys.,* 1998, **109**, 8218-8224.

40. K. Morokuma, *J. Chem. Phys.*, 1971, **55**, 1236-1244.

41. K. Kitaura and K. Morokuma, *Int. J. Quant. Chem.*, 1976, **10**, 325-340.

42. M. W. Schmidt, K. K. Baldridge, J. A. Boatz, S. T. Elbert, M. S. Gordon, J. H. Jensen, S. Koseki, N. Matsunaga, K. A. Nguyen, S. Su, et al., *J. Comput. Chem.,* 1993, **14**, 1347–1363.

43. W. J. Geary, *Coord. Chem. Rev.*, 1971, **7**, 81-122.

44. A. Golcu, M. Tumer, H. Demirelli and R. A. Wheatley, *Inorg. Chim. Acta*, 2005, **358**, 1785-1797.

45. P. R. Reddy and A. M. Reddy, *Proc. Indian Acad. Sci. (Chem. Sci.),* 2000, **112(6)**, 593-600.

46. H. Hamrit, S. Djebbar-Sid, O. Benali-Baitich, M. A. Khan and G. Bouet*, Synth. React. Inorg. Met.- Org. Chem.*, 2000, **30(10),** 1835-1848.

47. S. V. Sanap and R. M. Patil, *Research Journal of Pharmaceutical Sciences*, 2013, **2(1)**, 1-10.

48. K. Nakamoto, Y. Morimoto and A. E. Martell, *J. Am. Chem. Soc.,* 1961, **83**, 4528-4532.

49. P. R. Reddy, M. Radhika and P. Manjula, *J. Chem. Sci.*, 2005, **117(3)**, 239–246.

50. M. M. Mashaly, Z. H. Abd-Elwahab and A. A. Faheim, *J. Chin. Chem. Soc.*, 2004, **51**, 901–915.

51. S. A. Zabin and C. R. Jejurkar, *Asian J. Chem.*, 1995, **7(3)**, 542-550.

52. S. Kapoor and M. S. Sastry, *Proc. Indian Acad. Sci.* (*Chem. Sci.*), 2000, **112**, 459–463.

53. O. Zulbiye, Z. Huseyin and S. Mehmet*, Turk. J. Chem.*, 2011, **35**, 905–914.

54. E. L. S. Gomes and Jr. O. L. Casagrande, *Thermochim. Acta*, 1999, **331**, 87-91.

55. J. M. Berg and D. L. Merkle, *J. Am. Chem. Soc.,* 1989, **111**, 3759-3761.

56. N. C. Polfer, J. Oomens, D. T. Moore, G. von Helden, G. Meijer and R. C. Dunbar, *J. Am. Chem. Soc.,* 2006, **128**, 517–525.

57. S. G. Stepanian, I. D. Reva, E. D. Radchenko, M. T. S. Rosado, M. L. T. S. Duarte, R. Fausto and L. Adamowicz, *J. Phys. Chem. A,* 1998, **102**, 1041–1054.

58. K. Fukui, T. Yonezawa and H. Shingu, *J. Chem. Phys.,* 1952, **20**, 722–725.

59. M. T. Baei and S. Z. Sayyed-Alangi, *E-J Chem,* 2012, **9***,* 1244-1250.

60. C. L. Brooks III, M. Karplus and B. M. Pettitt, Proteins: a theoretical perspective of dynamics, structure, and thermodynamics. Wiley, New York, 1988.

61. M. Remko, D. Fitz and B. M. Rode, *J. Phys. Chem. A,* 2008, **112**, 7652–7661.

62. K. Wiberg, *Tetrahedron,* 1968, **24**, 1093-1096.

63. W. J. Hehre, L. Radom, P. v. R. Schleyer and J. A. Pople, Ab initio molecular orbital theory. Wiley, New York, 1986.

64. G. Das, *J. Mol. Model.*, 2013, **19**, 2981–2991.

65. S. Y. Lee and B. H. Boo, *J. Phys. Chem.,* 1996, **100**, 8782-8785.

66. K. Yokota, M. Hagimori, N. Mizuyama, Y. Nishimura, H. Fujito, Y. Shigemitsu and Y. Tominaga, *Beilstein J. Org. Chem.,* 2012, **8**, 266-274.

Table 1 Physical, conductivity and analytical data of the Ni(II), Cu(II) and Zn(II) complexes of L-Val. The calculated values of elemental analysis are given in square brackets and co-precipitation values are given in parentheses

Compound	Formula	Colour	F. W. (gm/mol)	M. Pt. (C^o)	Λ_M $\Omega^{-1}cm^2mol^{-1}$ (in DMSO)	Found (calc.) (%)		
						C	H	N
L-Val	$C_5H_{11}NO_2$	White	117.15	298	5.4	------	-------	------
Ni(L-Val)$_2$	$C_{10}H_{20}N_2O_4Ni$	Light Blue	290.97	315-330	6.7 (6.9)	41.31	6.70	9.55
						(41.25)	(6.79)	(9.61)
						[41.28]	[6.88]	[9.63]
Cu(L-Val)$_2$	$C_{10}H_{20}N_2O_4Cu$	Purplish	295.83	310-323	5.8 (6.0)	40.56	6.83	9.39
						(40.63)	(6.73)	(9.37)
						[40.60]	[6.81]	[9.47]
Zn(L-Val)$_2$	$C_{10}H_{20}N_2O_4Zn$	White	297.67	309-330	9.2 (9.7)	40.42	6.79	9.28
						(40.29)	(7.05)	(9.46)
						[40.35]	[6.77]	[9.41]

F.W=Formula weight

Table 2 Experimental and theoritical IR spectral data[a] of L-Val and its metal complexes prepared in solid state and by co-precepitation method (intensities are given in parentheses)

Compound			ν_{as}(N-H)	ν_s(N-H)	ν(O-H)	ν(C_2-H)	ν_{as} (COO^-)	ν_s(COO^-)	ν(C=O)	ν(C-N)	ν(C-O)	ν(M-O)	ν(M-N)	Δδ
L-Val	Expt.	A	3436	3133	------	2962	1598	1417	-------	1134	1271	------	------	181
	Calc.	C	3476 (8)	3390 (5)	3359 (270)	2919 (14)	------	------	1771 (313)	1115 (18)	1204 (20)	------	-------	-----
		D	3420 (111)	3345 (81)	------	3008 (30)	1639 (153)	1405 (25)	-------	1111 (108)	1286 (11)	------	-------	234
Ni(L-Val)$_2$	Expt.	A	3449	3263	-------	2957	1623	1414	-------	1116	1271	540	465s	209
		B	3447	3252	-------	2954	1611	1396	-------	1103	1270	542s	473w	215
	Calc.	C	3425 (30)	3353 (7)	-------	2936 (30)	1767 (1221)	1317 (6)	-------	1145 (416)	1264 (439)	555 (4)	488 (62)	450
		D	3430 (65)	3357 (29)	-------	2945 (44)	1688 (2062)	1338 (18)	-------	1151 (29)	1276 (501)	584 (0.5)	479 (82)	350
Cu(L-Val)$_2$	Expt.	A	3450	3291	-------	2955	1621	1394	-------	1096	1228	577s	469s	227
		B	3469	3298	-------	2923	1637	1387	-------	1114	1262	617s	477s	250
	Calc.	C	3437 (13)	3364 (15)	-------	2929 (54)	1759 (1180)	1315 (5)	--------	1147 (11)	1265 (431)	614 (6)	469 (37)	444
		D	3440 (62)	3367 (34)	-------	2939 (62)	1678 (1997)	1333 (677)	--------	1148 (321)	1280 (450)	539 (7)	465 (36)	345
Zn(L-Val)$_2$	Expt.	A	3446	3254	-------	2955	1611	1396	--------	1105	1271	542s	473w	215
		B	3448	3257	-------	2926	1637	1398	--------	1085	1278	567s	454s	209
	Calc.	C	3436 (29)	3362 (21)	-------	2942 (15)	1757 (1084)	1326 (93)	--------	1114 (354)	1287 (38)	551 (8)	468 (18)	431
		D	3448 (18)	3379 (32)	-------	2952 (11)	1659 (1823)	1351 (605)	--------	1169 (32)	1295 (15)	554 (8)	469 (14)	308

[a]Calculated at B3LYP/6-311++G(d,p); A=Solid state; B=Co-precipitation technique; C=Gas Phase; D=Solvent phase; w=weak; s=strong
For theoretical data: The frequencies below 1800 cm^{-1} are scaled with 1.01 and for those above 1800 cm^{-1} a correction factor 0.9679 is used.

Table 3 Experimental and calculated absorption maxima (λ_{max}) for all the reaction species

Systems	Experimentalλ_{max} in nm		Calculated calculated λ_{max} TD-B3LYP in nm			
	Solid state (DMSO)	Co-precepitation (DMSO)	Gas Phase		DMSO	
			Wave length	Oscillator Strength	Wave length	Oscillator strength
L-Val	261	268	216	0.01	210	0.016
Ni(L-Val)$_2$	270, 380, 624	280, 400, 632	610	0.0001	623	0.0003
Cu(L-Val)$_2$	269, 611	281, 617	576	0.0001	551	0.0001
Zn(L-Val)$_2$	274, 347,390	271, 359,405	257	0.0005	210	0.0001

Table 4 Fluorescence parameters of L-Val and its complexes in DMSO (intensities given in parentheses)

Compound	Excitation wavelength λ_{max} (nm)	Emission wavelength λ_{max} (nm)	Quantum yield (φf)	Stokes' shift (nm)
L-Val	261	337 (9998)	0.954	76
Ni(L-Val)$_2$	270	337 (2103)	0.544	67
Cu(L-Val)$_2$	269	335 (3070)	0.676	66
Zn(L-Val)$_2$	274	331 (3937)	0.752	57

Table 5 Maximum temperature values for decomposition along with corresponding weight loss values for solid state products

Compounds	Decomposition range (^{o}C)	Peak temperature (^{o}C)	Percentage weight loss (%)	Product expected	Residue state/colour	Mass changes Calc. (found)
Ni(L-Val)$_2$	218-339	328	75.77	NiO	Dark greenish powder	0.61 (0.57)
Cu(L-Val)$_2$	221-320	312	73.11	CuO	Brown powder	0.46 (0.46)
Zn(L-Val)$_2$	219-482	319	73.07	ZnO	White powder	0.91 (0.90)

Table 6 Calculated interaction enthalpies ΔH (kcal/mol) and Gibbs energies ΔG (kcal/mol); dipole moments (Debye); rotational constants (GHz) and HOMO/LUMO energy gaps (eV) for all the reaction species in gas and aqueous phase (aqueous phase values are given in parentheses)

Systems	ΔH	ΔG	Dipole Moments	Rotational Constants			HOMO/LUMO Energy gaps
				A	B	C	
L-Val	---	---	5.347 (12.922)	2.975 (2.815)	1.574 (1.614)	1.090 (1.163)	6.451 (6.567)
$Ni(L\text{-}Val)_2$	-80.23 (-66.36)	-74.74 (-64.18)	0.423 (0.580)	1.001 (0.992)	0.188 (0.187)	0.162 (0.162)	4.803 (4.840)
$Cu(L\text{-}Val)_2$	-43.50 (-52.17)	-38.87 (-47.58)	0.661 (1.144)	0.998 (0.986)	0.179 (0.179)	0.156 (0.156)	5.541 (6.029)
$Zn(L\text{-}Val)_2$	-44.82 (-27.33)	-41.07 (-26.49)	7.147 (11.469)	0.886 (0.866)	0.185 (0.180)	0.174 (0.172)	5.457 (6.373)

Table 7 Calculated bond lengths (in angstrom) and Wiberg bond indices of some structurally significant bonds of free L-Val and its metal complexes in gas and aqueous phase (aqueous phase values are given in parentheses)

Systems	L-Val	$Ni(L\text{-}Val)_2$	$Cu(L\text{-}Val)_2$	$Zn(L\text{-}Val)_2$	MD[a]
$C_2–C_1$	1.553 (1.567)	1.558 (1.548)	1.564 (1.554)	1.565 (1.555)	0.012 (0.019)
$C_2–C_3$	1.553 (1.546)	1.544 (1.547)	1.545 (1.548)	1.543 (1.546)	0.010 (0.002)
$C_2–N_6$	1.477 (1.517)	1.498 (1.495)	1.495 (1.492)	1.500 (1.490)	0.023 (0.027)
$C_3–C_4$	1.537 (1.539)	1.538 (1.538)	1.538 (1.538)	1.535 (1.535)	0.002 (0.004)
$C_1=O_8$	1.203 (1.242)	1.213 (1.225)	1.215 (1.228)	1.217 (1.233)	0.014 (0.017)
$C_1\text{-}O_7$	1.342 (1.264)	1.310 (1.303)	1.306 (1.298)	1.300 (1.289)	0.042 (0.039)
$M–O_7$	-----	1.847 (1.863)	1.912 (1.942)	1.923 (1.993)	-------
$M–N_6$	-----	1.918 (1.925)	2.029 (2.019)	2.114 (2.113)	-------
$*M–O_7$	-----	0.3676 (0.3404)	0.2096 (0.1824)	0.1807 (0.1468)	-------
$*M–N_6$	-----	0.3568 (0.3656)	0.1853 (0.1990)	0.1337 (0.1601)	-------

[a]Maximum deviation from L-Val; *Wiberg bond indices

Table 8 Calculated bond angles (in degrees) of free L-Val and its metal complexes in gas and aqueous phase (aqueous phase values are given in parentheses)

Bond Angles	L-Val	$Ni(L\text{-}Val)_2$	$Cu(L\text{-}Val)_2$	$Zn(L\text{-}Val)_2$	MD[a]
$N_6–C_2–C_1$	107.4 (104.4)	106.2 (106.1)	107.0 (107.1)	111.5 (111.1)	4.1 (6.7)
$N_6–C_2–C_3$	116.3 (109.5)	114.0 (114.2)	114.3 (114.5)	113.7 (113.7)	2.6 (5.0)
$C_1–C_2–C_3$	113.5 (114.5)	115.9 (115.7)	115.1 (115.1)	112.0 (112.7)	2.4 (1.2)
O_8-C_1-O_7	122.1 (128.7)	124.5 (123.3)	124.7 (123.6)	125.7 (124.3)	3.6 (5.4)
C_2-C_1-O_7	113.3 (114.4)	113.4 (114.1)	114.1 (114.9)	116.8 (117.5)	3.5 (3.1)
C_2-C_1-O_8	124.6 (116.9)	122.1 (122.5)	121.1 (121.4)	117.5 (118.1)	7.1 (5.6)
$H_a–N_6–C_2$	111.4 (114.3)	110.4 (110.5)	110.5 (110.6)	110.1 (110.7)	1.3 (3.8)
$H_b–N_6–C_2$	111.9 (102.2)	112.7 (111.5)	112.7 (111.5)	110.9 (110.9)	1.0 (9.3)
$H_a–N_6–H_b$	107.5 (110.8)	106.4 (106.5)	106.3 (106.5)	105.7 (106.2)	1.8 (4.6)
C_2-C_3-C_4	111.4 (111.2)	111.9 (111.9)	112.1 (112.2)	111.9 (111.5)	0.7 (1.0)
C_2-C_3-C_5	111.7 (112.2)	111.0 (111.0)	110.9 (110.8)	112.5 (112.8)	0.8 (1.4)
C_4-C_3-C_5	109.5 (109.8)	109.7 (109.4)	109.6 (109.3)	111.7 (111.4)	2.2 (1.6)

[a]Maximum deviation from L-Val

Table 9 Calculated dihedral angles (in degrees) for free L-Val and its metal complexes using B3LYP level of theory in gas and aqueous phase (aqueous phase values are given in parentheses)

Dihedrals	L-Val	$Ni(L\text{-}Val)_2$	$Cu(L\text{-}Val)_2$	$Zn(L\text{-}Val)_2$	MD[a]
N_6-C_2-C_1-O_7	20.3 (-22.3)	24.3 (23.8)	29.2 (27.6)	10.8 (11.0)	8.9 (5.3)
N_6-C_2-C_1-O_8	-161.4 (157.7)	-157.6 (-158.1)	-152.7 (-154.5)	-171.6 (-171.5)	10.2 (13.8)
O_7-C_1-C_2-C_3	150.3 (97.4)	151.8 (151.7)	157.4 (156.2)	139.6 (140.0)	10.7 (58.8)
C_1-C_2-C_3-C_4	-168.0 (176.9)	-167.5 (-165.8)	-166.5 (-164.5)	168.2 (168.9)	1.5 (12.4)
C_1-C_2-C_3-C_5	69.2 (53.5)	69.5 (71.7)	70.6 (73.0)	-65.2 (-64.8)	4.0 (19.5)
N_6-C_2-C_3-O_4	-42.7 (-66.3)	-44.0 (-42.1)	-42.1 (-39.8)	-64.2 (-63.4)	21.5 (26.5)
N_6-C_2-C_3-O_5	-165.5 (170.3)	-167.0 (-164.6)	-165.0 (-162.3)	62.5 (62.8)	103.0 (107.5)

[a]Maximum deviation from L-Val

Figure captions

Fig. 1 Schematic representation of the chemical structures of L-Val and its metal complexes

Fig. 2 Electronic absorption spectra of L-Val and its metal complexes in DMSO

Fig. 3 Fluorescence spectra of L-Val and its metal complexes in DMSO

Fig. 4 EDAX spectrum of the $Cu(L\text{-}Val)_2$ complex prepared in solid state

Fig. 5 SEM morphology of the $Cu(L\text{-}Val)_2$ complex prepared in solid state

Fig. 6 TEM morphology of the $Cu(L\text{-}Val)_2$ complex prepared in solid state

Fig. 7 Optimized structures of L-Val and its metal complexes in aqueous phase

Fig. 8 The 3D plots of HOMO and LUMO of the metal complexes in aqueous phase

Fig. 9 The molecular electrostatic potentials mapped on the electron density surface in L-Val and its metal complexes in aqueous phase

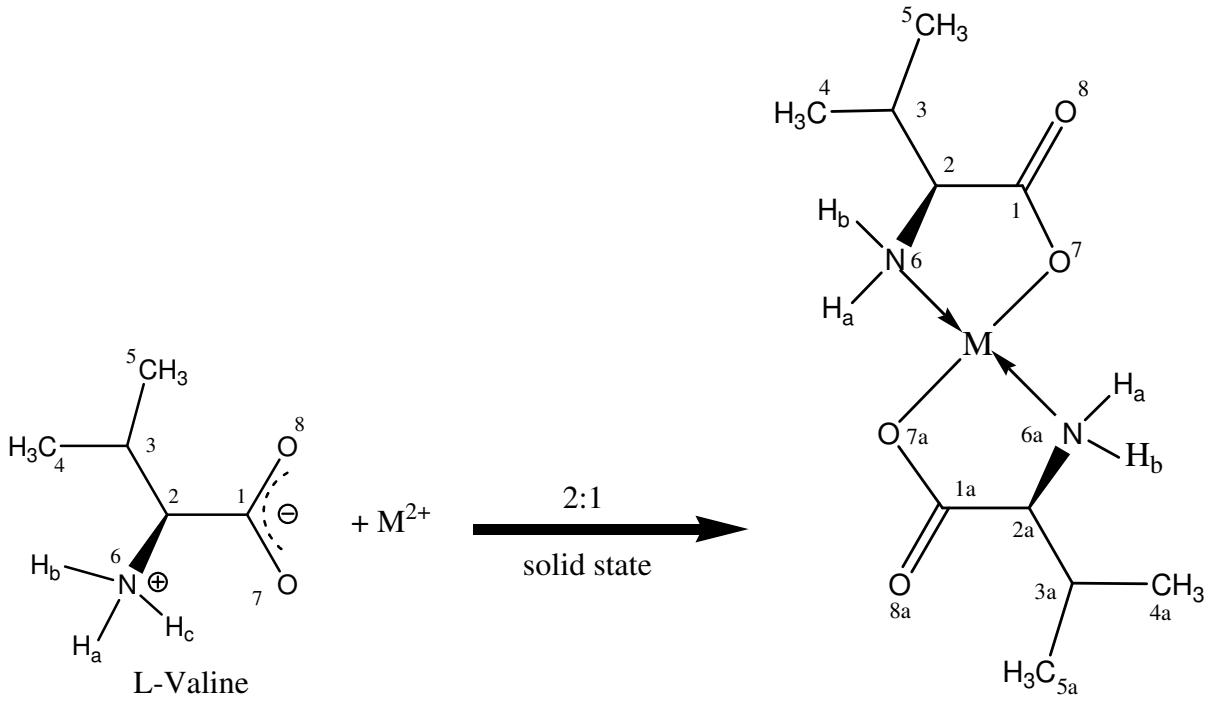

Fig. 1 Schematic representation of the chemical structures of L-Val and its metal complexes

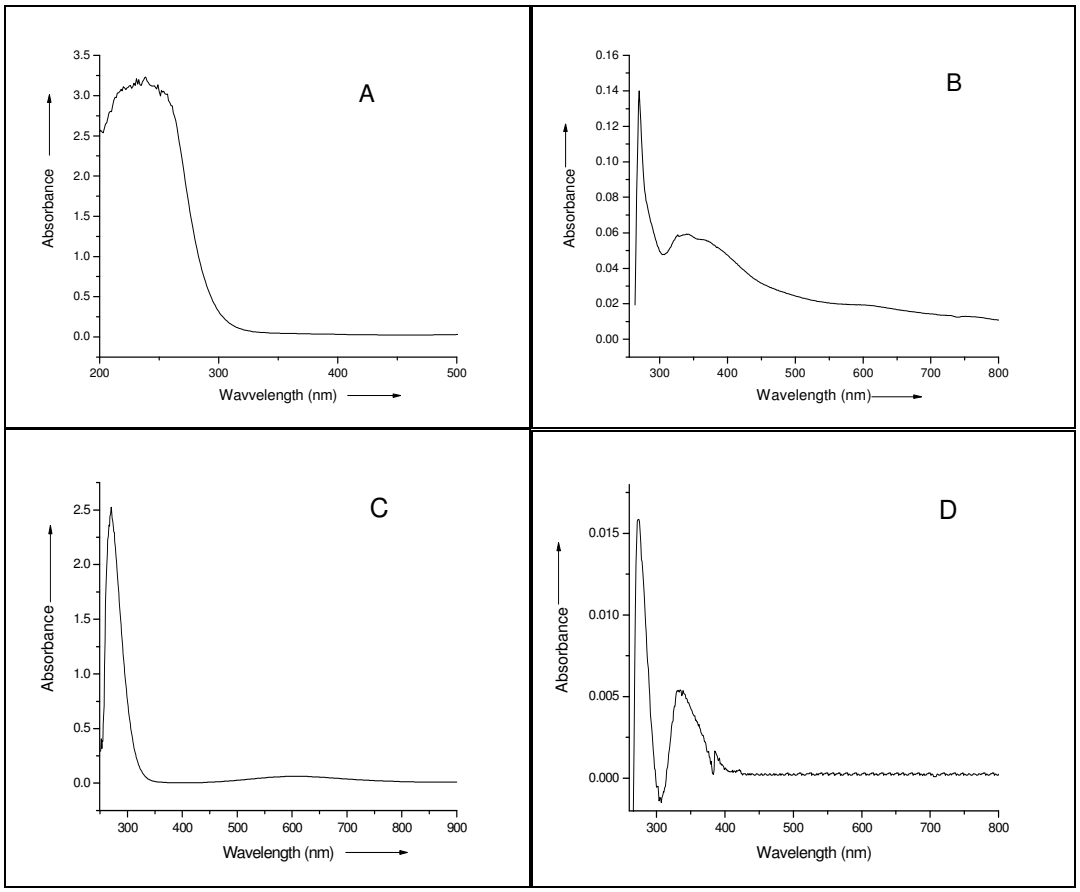

Fig. 2 Electronic absorption spectra of L-Val and its metal complexes in DMSO
A) L-Val; B) $Ni(L\text{-}Val)_2$; C) $Cu(L\text{-}Val)_2$; D) $Zn(L\text{-}Val)_2$

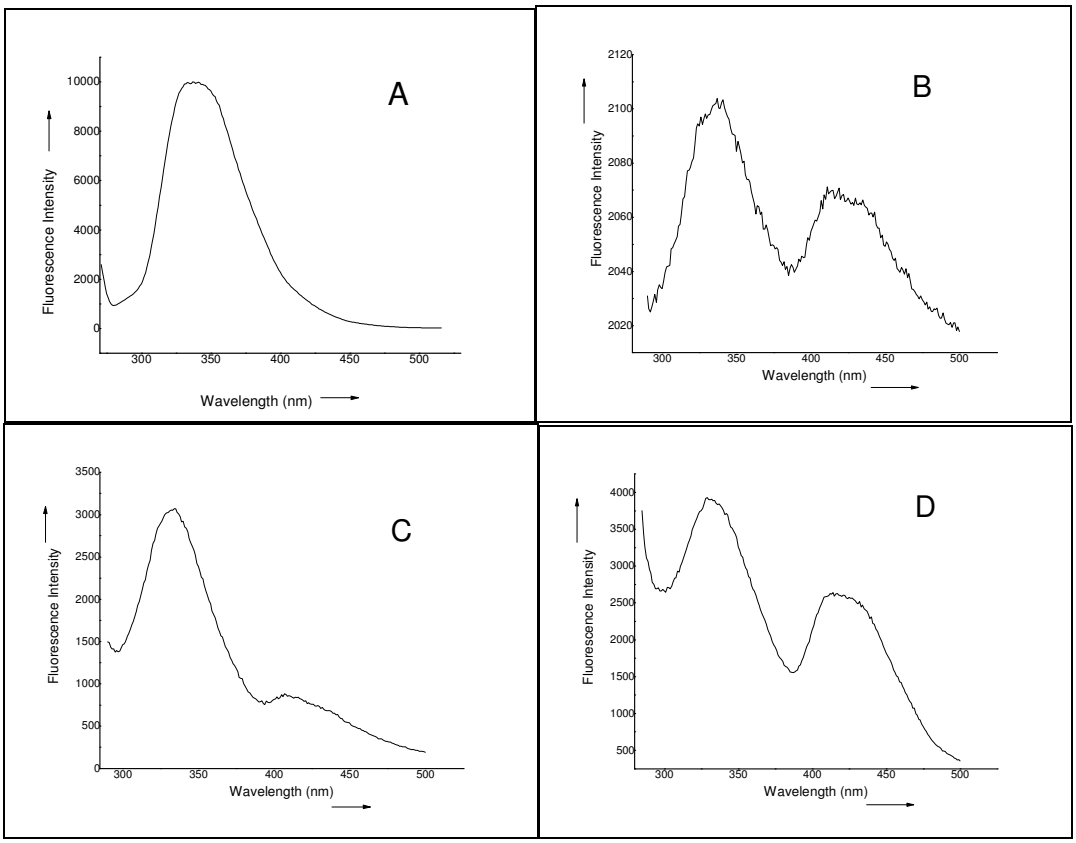

Fig. 3 Fluorescence spectra of L-Val and its metal complexes in DMSO
A) L-Val; B) Ni(L-Val)$_2$; C) Cu(L-Val)$_2$; D) Zn(L-Val)$_2$

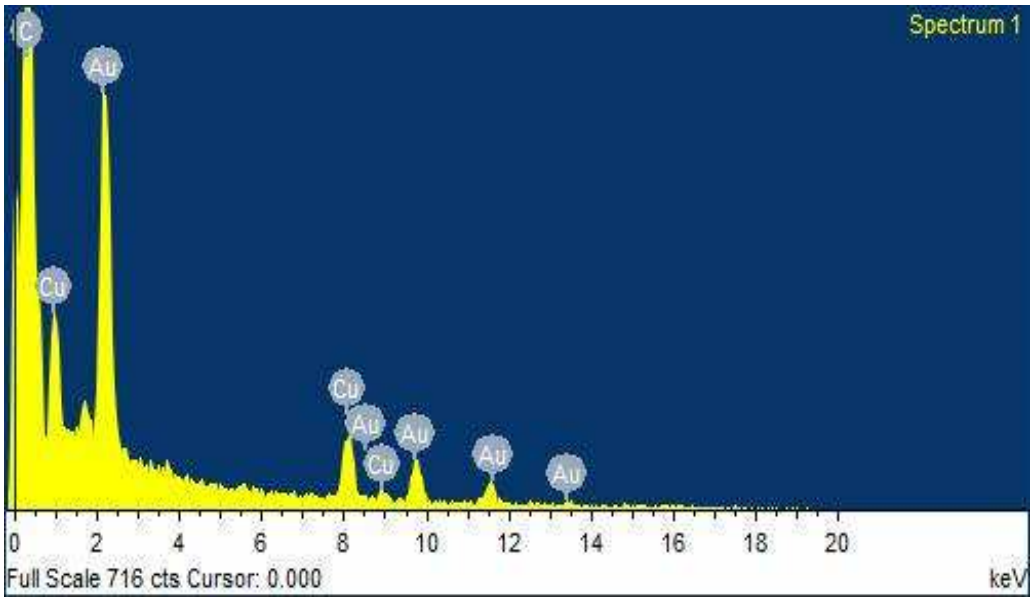

Fig. 4 EDAX spectrum of the Cu(L-Val)$_2$ complex prepared in solid state

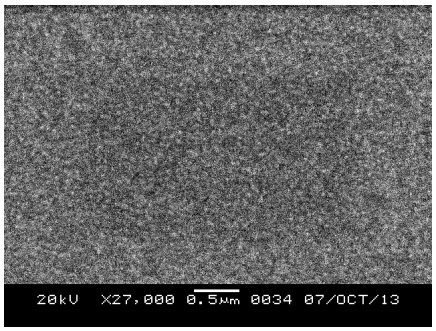

Fig. 5 SEM morphology of the Cu(L-Val)$_2$ complex prepared in solid state

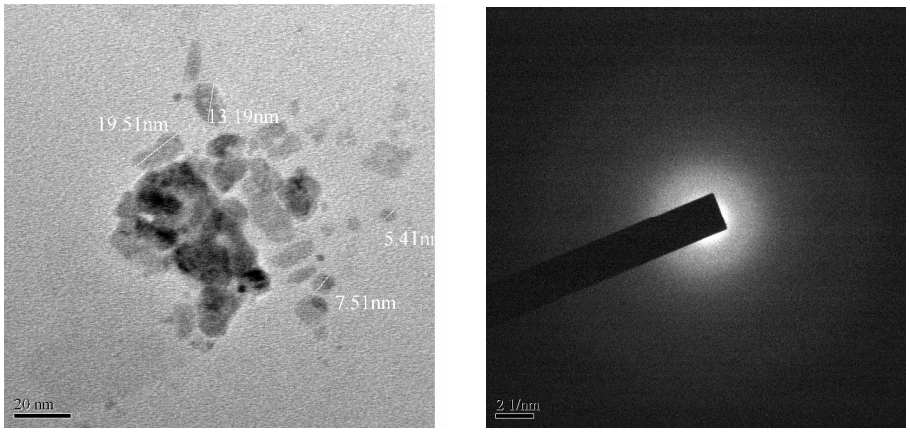

Fig. 6 TEM morphology of the Cu(L-Val)$_2$ complex prepared in solid state

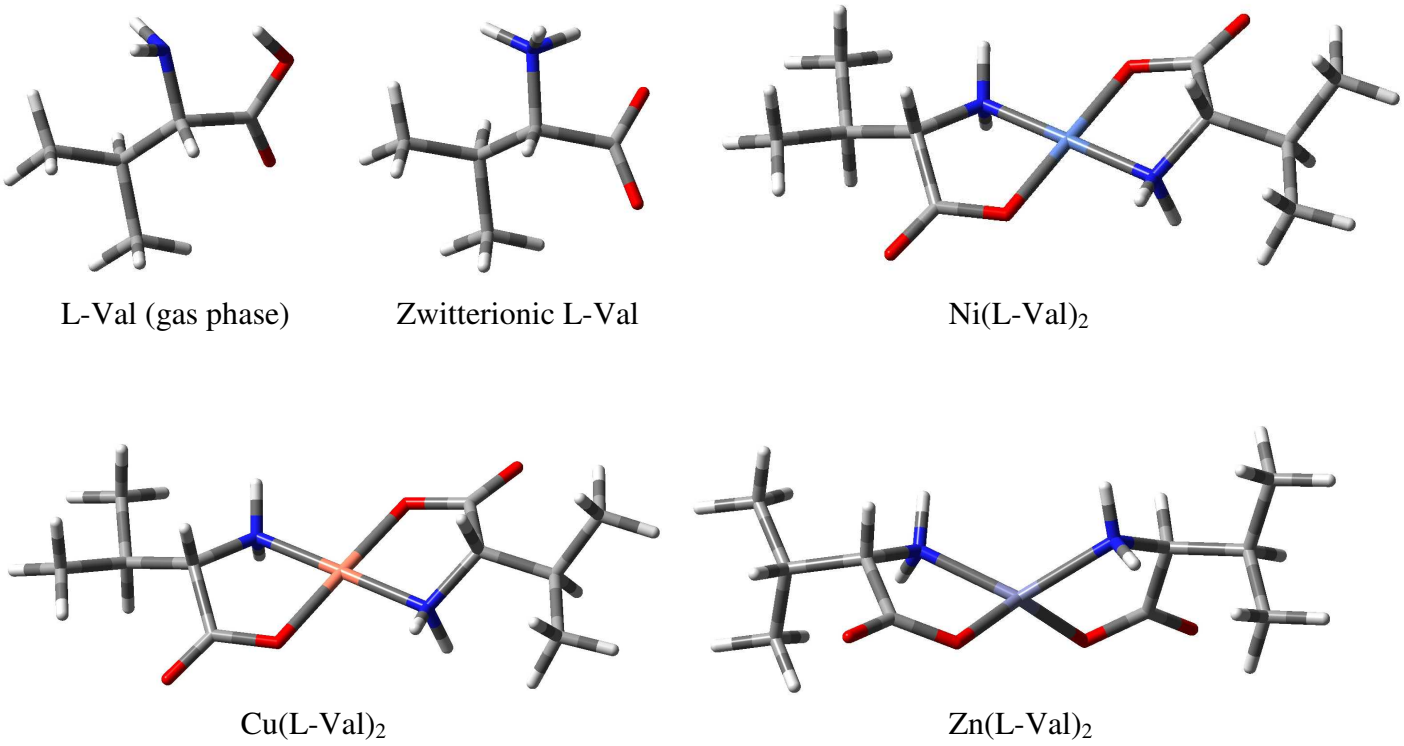

Fig. 7 Optimized structures of L-Val and its metal complexes in aqueous phase

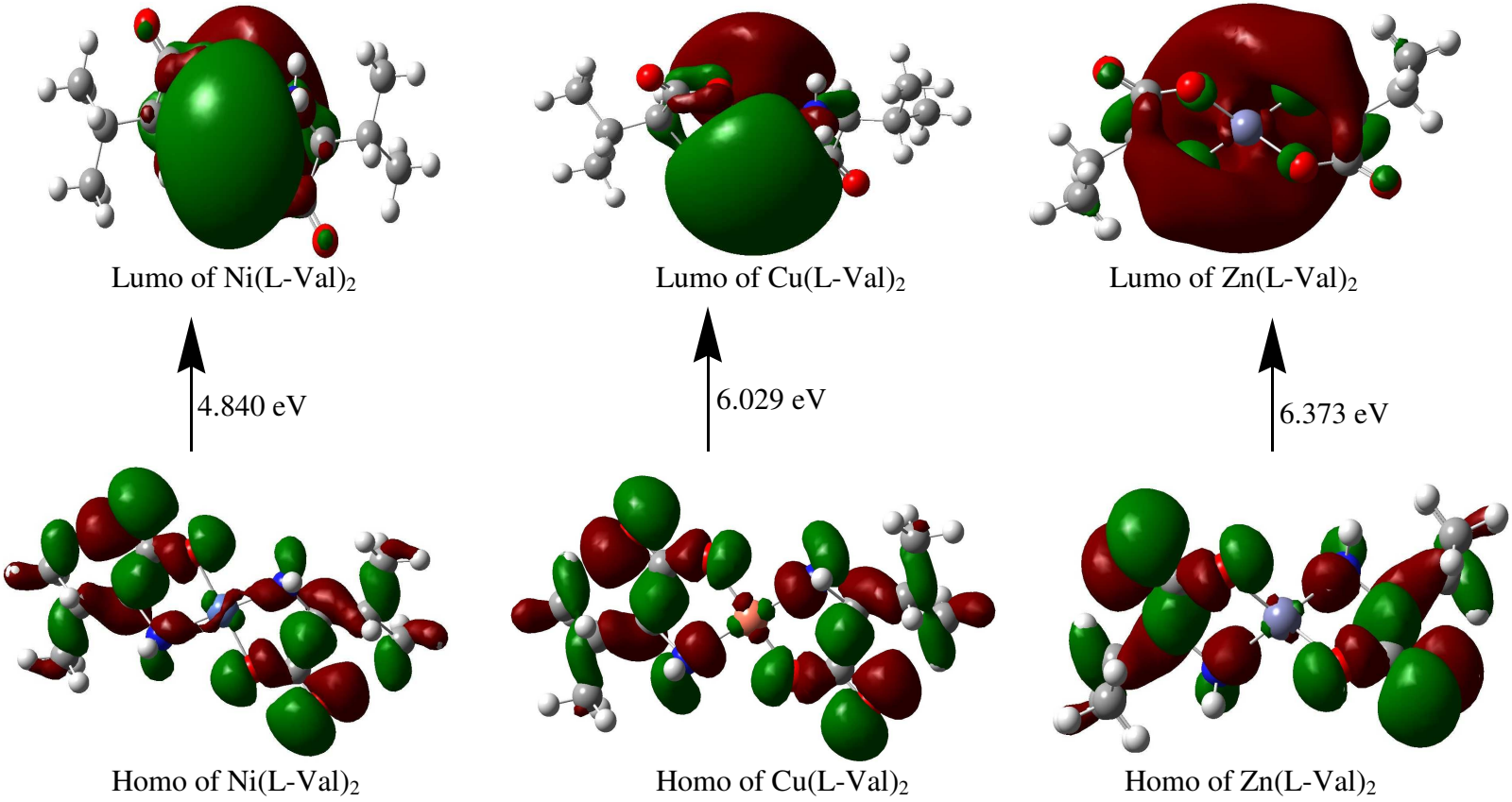

Fig. 8 The 3D plots of HOMO and LUMO of the metal complexes in aqueous phase

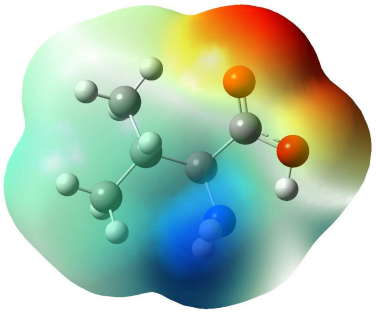

L-Val (Gas)

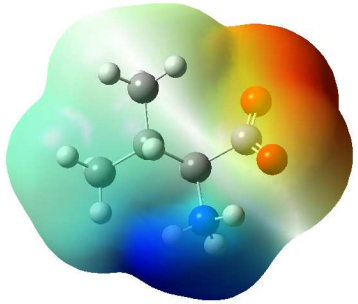

L-Val (Aqueous)

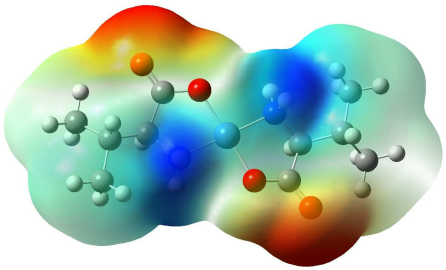

$Ni(L\text{-}Val)_2$

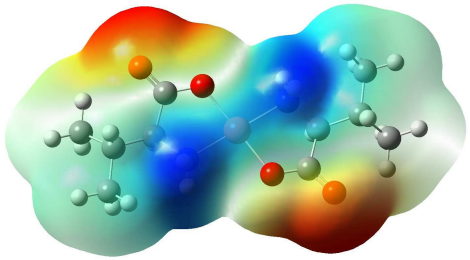

$Cu(L\text{-}Val)_2$

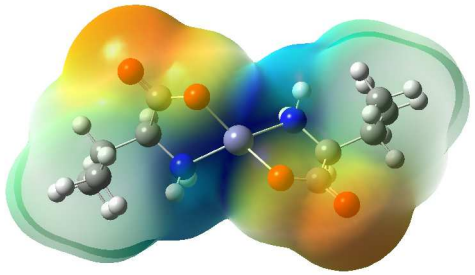

$Zn(L\text{-}Val)_2$

Fig. 9 The molecular electrostatic potentials mapped on the electron density surface in L-Val and its metal complexes in aqueous phase

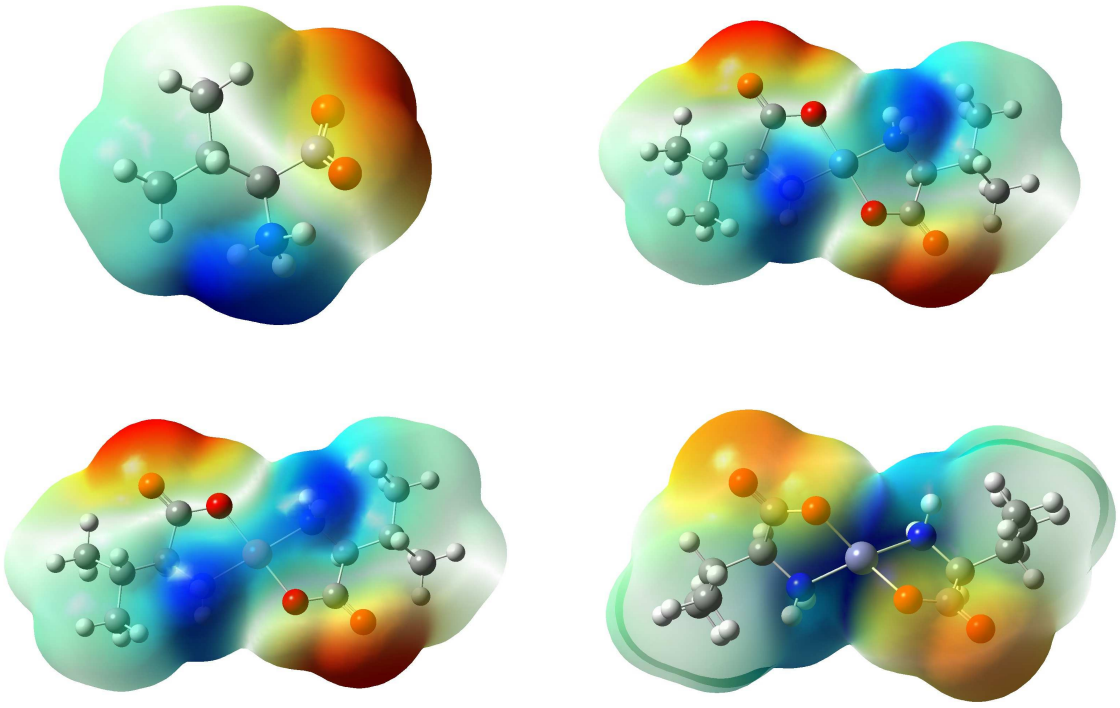

Molecular electrostatic potentials in L-Val and its metal complexes